Autonomous Photovoltaic Water Pumping System

Ahmed A. A. Hafez
Electrical Engineering Department, Faculty of Engineering, Assiut University, Assiut, Egypt,
PO 71516 elhafez@aun.edu.eg

***Abstract*- This paper proposes simple, efficient and reliable autonomous PV water pumping system. The system operation under normal/abnormal conditions was investigated by thoroughly mathematical and simulation work.**

Key words: PV water pumping, Centrifugal pump, DC/DC choppers, Faults

I. INTRODUCTION

Water resources are indispensable for social and economic development. The need for developing eco-friendly technology for provision of the drinking water is mandatory. The Photovoltaic (PV) water pumping systems are the key technology, as energy independence and environmental compatibility are two distinguishable features of PV systems [1-6]. Furthermore, PV water pumping systems have the advantages of: reliability, low maintenance, eco-friendly, reduced installation and running costs, and the matching between the power generated and the water usage need. The water tanks are preferred storage option in PV pumping systems instead of batteries [7-12].

For best utilization, PV water pumping systems have to operate at their maximum power point (MPP). However, the MPP varies with the insolation, temperature and other ageing effects. Numerous MPP Tracking (MPPT) techniques were reported in the literature [1-12]. These methods vary in complexity, cost, sensors requirements, convergence speed, and range of effectiveness, availability, and implementation hardware [1-6]. A simple and efficient MPPT is given in [6]. This technique emerged from the approximately linear relationship between the PV module short circuit and maximum power point currents at different climatological conditions. The current at maximum power is claimed in [6] to vary from 0.78 to 0.92 times the short-circuit current. This technique is well suited for the boost topology, as the short circuit current is extracted from the switch current during on-state. Therefore, no power loss is resulted from employing this method [6].

Recently research efforts [7-12] are drafted to design and analyze the performance of PV water pumping for residential and agriculture applications. For example, Ref. [8] concluded that a DC motor driving a centrifugal pump is a well-matched load for a PV array; as this system absorbs most PV array power. In [9] a load composed of a DC motor driving a constant volume pump was investigated. This system, as claimed in [9], is not suited for PV, as the motor driving a constant volume pump requires approximately constant current. In [10] the steady-state and starting performance of different DC motors and water pumps directly coupled to a PV array were analyzed; the study concluded that permanent magnet (separately excited) DC motor driving centrifugal pump is the best match for PV array.

In the studies mentioned before [7-12], models were developed for investigating the performance of the motor, pump and MPPT. The complicated non-linear relationship between these models requires sophisticated numerical skills. Moreover, these studies were not paying attention to the faultly mode of the system operation.

In this paper, simple and efficient PV directly coupled water pumping system is proposed. A boost DC-DC chopper interfaces the motor-pump to the PV generator. The boost extracts maximum power from PV generator at different irradiation /temperature levels. The paper addresses also system operation under faults in PV panel/boost circuit.

II. SEYSTEM DSCRIPTION

The system under study, Fig. 1, is composed of PV generator, pumping system and DC-DC chopper. In the following, detailed modeling for different system components is given.

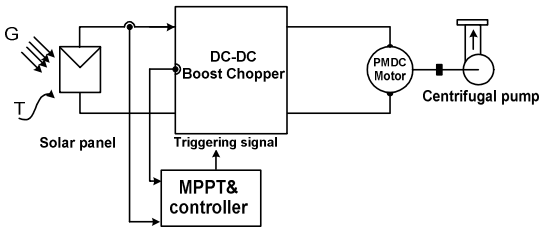

Fig. 1. Stand-alone PV water pumping system

A. PV Generator

The PV generator, as shown in Fig. 2, is modeled as solar irradiation and temperature dependent current source I_{ph} in parallel with diode and shunt resistance R_{sh}. This combination is in series with a series resistance R_s [4].

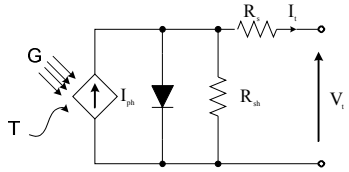

Fig. 2. Equivalent circuit of PV generator

The relation between the terminal current I_t and voltage V_t of a PV generator is expressed by,

$$I_t = I_{ph} - I_o \left(e^{\frac{V_t + I_t R_s}{V_{th}}} - 1 \right) - \frac{V_t + I_t R_s}{R_{sh}} \quad . \qquad (1)$$

where I_o is the diode saturation current. The PV generator is consisting of two series connected Kyocera KC200GT solar panel. Each KC200GT panel is composed of 54 series connected cell, the parameters of KC200GT module are given in Table 1 [5] .

TABLE I
PARAMETERS OF KC200GT SOLAR MODULE AT 25°C AND 1000W^{2}m^{-2}[5]

No. of cells	54
Short circuit current	8.21A
Open circuit voltage	32.9V
Current at MPP	7.61A
Voltage at MPP	26.3V
Maximum power	200.143W
Voltage coefficient	-0.1230V/K
Current coefficient	0.0032A/K

The values of shunt resistance R_{sh} and series resistance R_s calculated by iterative method in [4] are 415.405Ω and 0.221Ω respectively. The power-voltage curves of the PV generator calculated at 25°C and different irradiation levels are given in Fig. 3.

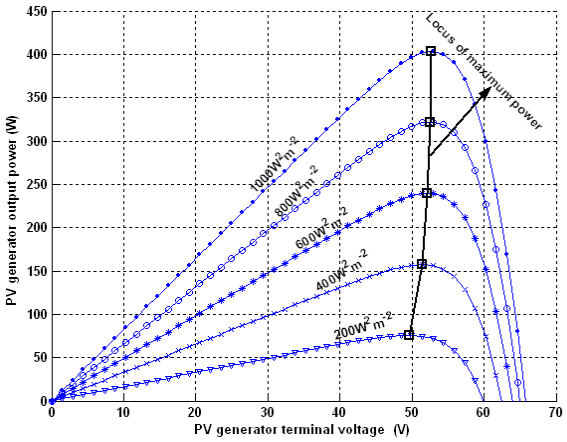

Fig. 3. Power versus voltage of PV generator at 25°C for different irradiation levels, locus of maximum power (black)

Fig. 3 shows that the voltage at maximum power is less dependent on solar irradiance. As, the voltage reduction is only 4.9%, (1.5V), for 80% drop in the solar irradiance and output power.

B. Pumping System

The pumping system is composed of Permanent Magnet DC motor (PMDC) coupled with centrifugal pump.

1. PMDC motor

The dynamic performance of the PMDC motor is predicated by the following set of equations.

$$\frac{di_a}{dt}=\frac{1}{L_a}\left(V_a-R_aI_a-k_\Phi\omega\right) \quad (2)$$

$$\frac{d\omega}{dt}=\frac{1}{j_a}\left(k_\Phi I_a-T_L-B\omega\right) \quad (3)$$

I_a, V_a, ω, R_a, B, K_Φ are motor current, voltage, speed, resistance, friction coefficient and the back emf constant. The parameters of the PMDC are given in Table 2.

2. Centrifugal Pump

The centrifugal pumps are usually preferred for PV water pumping systems due to their simplicity, availability in a wide range of flow rates and heads, elevated operating efficiency and reduced cost [7, 8].

TABLE 2
PARAMETERS OF PMDC MOTOR

Motor hp	½
Rated voltage	110V
Rated armature current I_{arated}	3.5A
Rated speed	1260rpm
Back emf constant k_Φ	0.8 V. sec.rad^{-1}
Armature resistance R_a	1.2Ω
Armature inductance L_a	0.2H
Moment of inertia J_a	0.025 Nm.rad^{-1}
Friction coefficient B	0.0

The performance of centrifugal pump generally is predicted by using affinity laws, which associates pump flow Q rate and power P to head H and speed ω provided that the pump efficiency remains constant over speed variations[7].

$$\frac{Q}{Q_{ref}}=\frac{\omega}{\omega_{ref}} \quad (4)$$

$$\frac{H}{H_{ref}}=\left(\frac{\omega}{\omega_{ref}}\right)^2 \quad (5)$$

$$\frac{P}{P_{ref}}=\left(\frac{\omega}{\omega_{ref}}\right)^3 \quad (6)$$

Q_{ref}, $H_{ref,}$ and $P_{ref,}$ are the reference flow rate, head and power at the reference speed ω_{ref}. Sophisticated models for the centrifugal pump and motor are used in [10-12]. Here in this study the pump is assumed lossless; therefore the driving torque of the pump is modeled by,

$$T_L=k_m\omega^2 . \quad (7)$$

The value of the constant k_m is selected for medium size pump.

The relation between motor speed ω/flow rate Q and PV generator terminal voltage V_t under steady-state conditions can be obtained by assuming lossless DC-DC chopper. Accordingly the PV module power is equal to motor input power.

$$V_tI_t=k_\Phi\omega I_a+R_aI_a^2 \quad (8)$$

The terminal voltage V_a and motor current I_a are related to PV generator terminal voltage V_t, current I_t and duty cycle D respectively by $V_t/(1-D)$, and $I_t(1-D)$. Substituting these relations into (8), the motor speed is given by,

$$\omega=\frac{V_t}{k_\Phi(1-D)}-\frac{R_aT_L}{k_\Phi^2} . \quad (9)$$

Substituting (7) into (9) and solving for motor speed,

$$\omega\approx\sqrt{\left(\frac{V_t}{1-D}\right)\left(\frac{k_\Phi}{R_ak_m}\right)}=\sqrt{V_a\left(\frac{k_\Phi}{R_ak_m}\right)} . \quad (10)$$

Equation (10) predicts that the speed and flow rate are minimum for D=0. This situation resembles permanent opening of the boost switch, which may attribute to faults in the gate circuit or the switch.

C. DC-DC Boost Converter

The non-isolated boost topology is used for coupling the PV generator to the pumping system due to:

1. The boost converter allows always tracking of maximum power point irrespective of solar irradiance level, due to its intrinsic characteristics.
2. The diode in the boost converter protects the PV module from damage under shading condition or failure in the pumping system.
3. The input inductor ensures continuous input current with minimum ripple level, which has the advantages of reducing loss and hence increasing the captured power from the PV module.
4. The position of the boost switch allows the using of an efficient, simple and cheap MPP, which is fractional short circuit current[6].
5. The input and output have common ground, which reduces the complexity of the control circuit.

The components of the boost converter are designed for 5% ripple in the PV generator terminal current and armature voltage of PMDC. The values of the input inductor and output capacitor are given in Table 3.

TABLE 3
PARAMETERS OF BOOST CONVERTER

Boost input inductor L_s	8.6mH
Boost output capacitor C_{out}	50μF

Assuming continuous mode conduction of inductor current, the dynamic performance of the boost converter averaged over a switching cycle is expressed by,

$$\frac{dI_t}{dt}=\frac{V_t-(1-d)V_a}{L_t}, \qquad (11)$$

$$\frac{dV_a}{dt}=\frac{I_t(1-d)}{C_o}-\frac{I_a}{C_o}. \qquad (12)$$

C. MPPT

Generally, there is a linear relation between short-circuit I_{sc} and maximum power point I_{max} current in PV modules [5-6]. The short-circuit I_{sc} and maximum power point I_{max} currents are plotted in Fig. 4 for Kyocera KC200GT at different levels of solar irradiation/temperature. The value of short circuit current I_{sc} is determined by sensing the switch current of the boost chopper during the on-state[6].

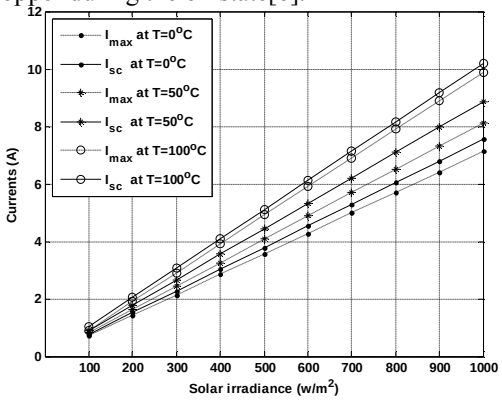

Fig. 4. Short circuit I_{sc} (solid) and maximum power point I_{max} (dotted) currents for different levels of solar irradiance at 0°C (point),50°C(star) and 100°C(circle)

Fig .4 shows that both short-circuit I_{sc} and maximum power point I_{max} currents vary linearly with solar irradiance; and the current I_{max} can be calculated by $I_{max}=k_{pv}*I_{sc}$, particularly at high irradiation/temperature levels. For Kyocera KC200GT, Fig. 4, the gain k_{pv} is 0.91. This value is considered to be a good comprise for different levels of solar irradiance and temperature.

III. CONTROLLER TUNING

Fig. 5, shows the equivalent circuit of the whole system. The value of short circuit current of PV generator is extracted from the sensed switch current, and then multiplied by the gain k_{pv} to synthesize the reference value. The current of the PV generator is compared with the reference; a PI compensator forces the system to operate at MPP.

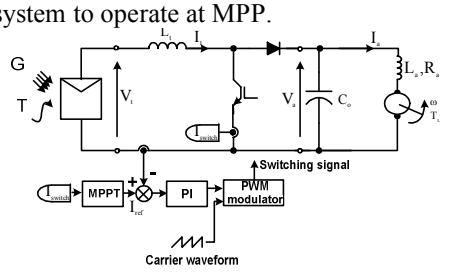

Fig. 5 Equivalent circuit of PV generator, DC/DC boost and PMDC

Perturbing equations (1)-(3), (7) and (11)-(12) around steady-state operating point, the transfer function between the PV generator terminal current and switch duty cycle is given by,

$$\frac{\Delta I_{in}}{\Delta d}=G_d(s)=\frac{a_3s^3+a_2s^2+a_1s+a_o}{b_4s^4+b_3s^3+b_2s^2+b_1s+b_o} \qquad (13)$$

where the parameters a_3, a_2, a_1, a_o, b_4,b_3,b_2,b_1 and b_o are given in the Appendix . The parameters a_3-a_o and , b_4-b_o are positive irrespective of the operating point, thus the transfer function G_d has four poles and three zeros all in the left hand plane. The response of G_d at different frequencies is shown in Fig. 6.

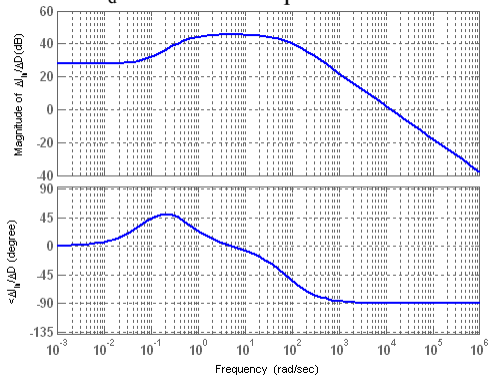

Fig. 6. Open loop frequency response of G_d

Fig. 6, shows that the transfer function G_d has a high gain and three combinations of pole-zero cancellation. The first combination is at very low frequency, while the second and the third are at low and high frequencies respectively. The transfer function is dominated by a pole at 73rad/sec. This pole is found to be dependent on the boost inductor.

The PI compensator C_d is tuned such that the system has fast dynamic response and adequate attenuation for switching ripples. This is realized by placing the controller zero over the

boost inductor pole, while the gain is selected to provided the desired bandwidth. The parameters of the PI compensator are given in Table 4.

TABLE 4
PARAMETERS OF PI COMPENSSATOR

k_c	40
z_c	0.01

The frequency response of $G_{d*}C_d$ transfer function is shown in Fig. 7.

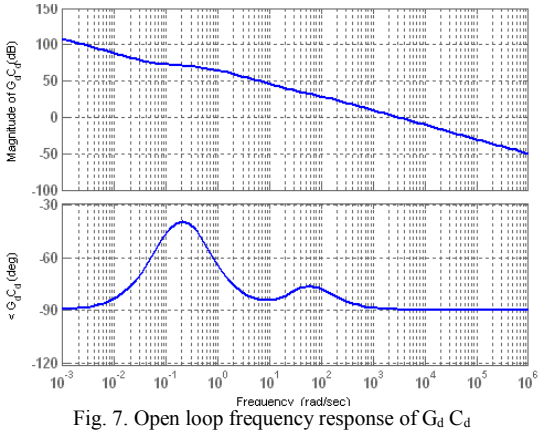

Fig. 7. Open loop frequency response of G_d C_d

Fig. 7, shows that the system has a sufficient high bandwidth of around 5600(rad/sec), and a phase margin of around 88°. This high bandwidth has the advantage of almost instantaneously reference current tracking. The closed loop frequency response of $\Delta I_l/\Delta I_{ref}$ is shown in Fig. 8.

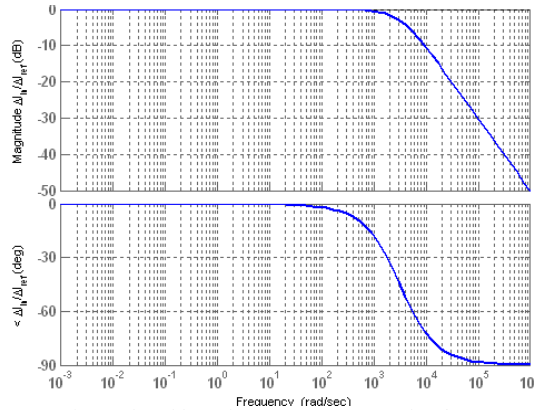

Fig. 8. closed loop frequency response of $\Delta I_l/\Delta I_{ref}$

Fig. 8 shows that the controller provides adequate attenuation for switching frequency ripples. Moreover, it maintains the system stability at wide range operating points.

The dynamic performance of system for stepped solar irradiance is shown in Figs. 9-10. In these Figures the solar irradiance is abruptly stepped from $1000W^2m^{-2}$ to $400W^2m^{-2}$ at 4 seconds and stepped from $400W^2m^{-2}$ to $800W^2m^{-2}$ at 6.5 seconds.

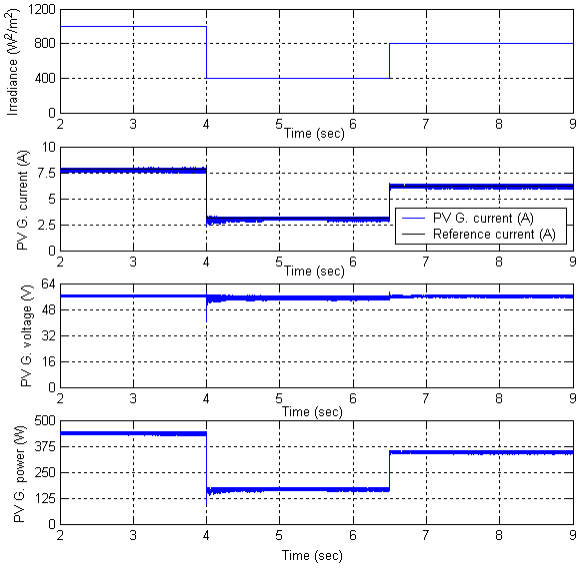

Fig. 9. Solar irradiance (top graph), PV generator current and reference current (first middle), PV generator terminal voltage (second middle), PV generator power (bottom graph) for different levels of solar irradiance at 25ºC

The instantaneous tracking of PV generator current to I_{max} is apparent in Fig. 9. This is attributed to the high bandwidth of the controller, as mentioned before. The PV generator voltage drops around 2V, when the solar irradiance is stepped from $1000W^2m^{-2}$ to $400W^2m^{-2}$. This matches the results in Fig. 3. The PV generator power varies almost linearly with the solar irradiance, as it drops from 400w to 152w for 60% drop in the solar irradiation.

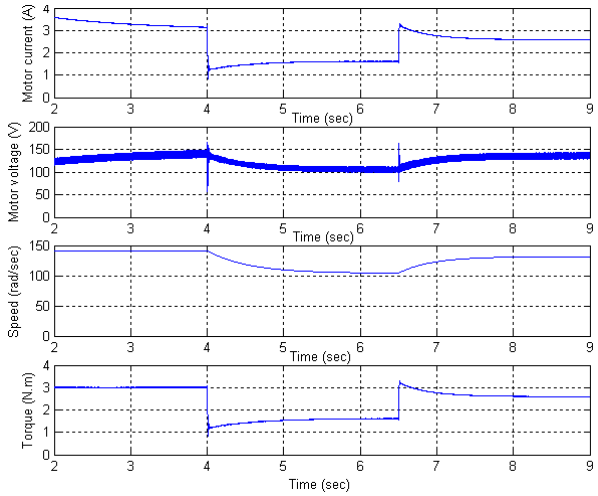

Fig. 10. Motor current (top graph), voltage (first middle), speed (second middle), and electromagnetic torque (bottom graph) for different levels of solar irradiance at 25ºC

Fig. 10, shows that the speed of PMDC motor varies with the motor terminal voltage as predicted in (10). The spikes in the motor terminal voltage, Fig. 10, during solar irradiance abrupt change are attributed to armature inductance.

IV. FAULTED MODE OF BOOST SWITCH

If the boost switch, Fig. 4, encounters a short-circuit fault, the PV power drops to zero and hence the water flow.

However, water flow continues for a while that depends on the value of output capacitance, voltage and stored charge.

The situation is different under switch open-circuit/gating signal fault. For this condition, the system continues to function albeit at reduced power and hence water flow rate. Water flow is a good prognostics factor, as under short-circuit fault the water flow will cease, whereas it continues for open-circuit fault albeit at reduced level.

The system operation under open-circuit switch fault is additional advantages for boost topology. The operating point of the system could be determined from intersection of PV generator I-V characteristics and that of pumping system, Fig. 10.

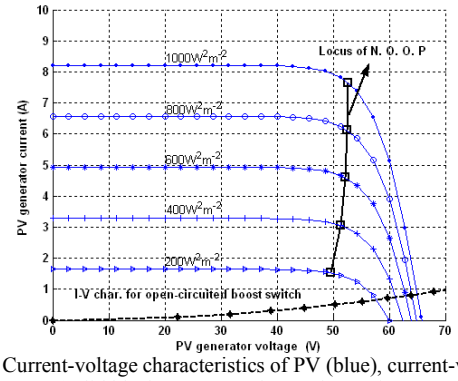

Fig. 10. Current-voltage characteristics of PV (blue), current-voltage at maximum power (solid black) current-voltage of pumping system under O.C fault (dashed black) at different solar irradiations and 25°C

Under open-circuit condition the captured power drops to 7.5% of maximum power at $1000W^2m^{-2}$ and 25°C. This power could be boosted by using a PMDC motor with small rated voltage. The dynamic performance of system under open-circuited boost switch for stepped solar irradiance is shown in Figs.11-12.

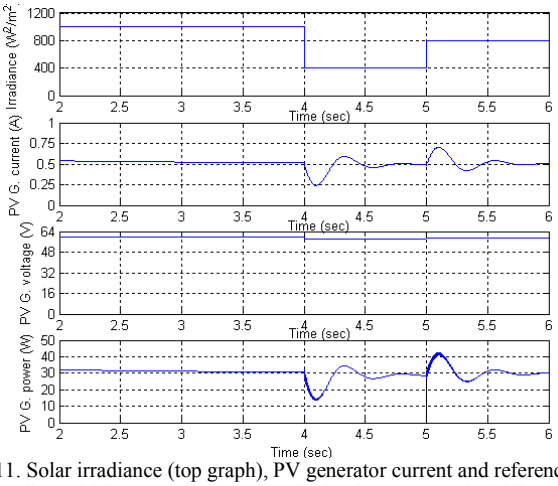

Fig. 11. Solar irradiance (top graph), PV generator current and reference current (first middle), PV generator terminal voltage (second middle), PV generator power (bottom graph) for different levels of solar irradiance at 25°C

Fig. 11, shows that the variations in the solar irradiance have insignificant impact on the PV terminal voltage even at open-circuit switch fault. The PV generator current/power in Fig. 11 agrees with those in Fig. 10.

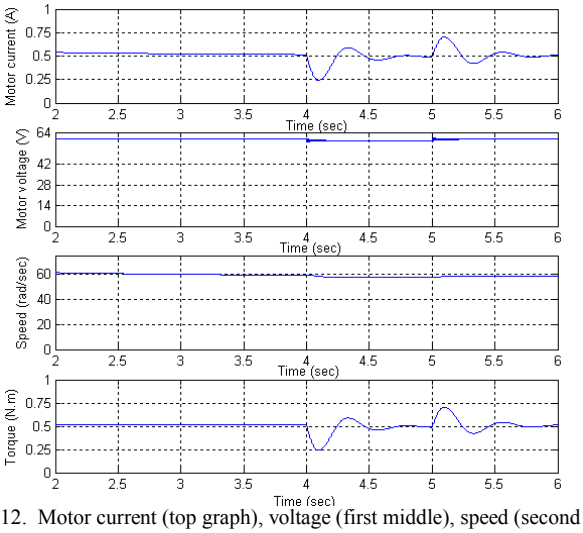

Fig. 12. Motor current (top graph), voltage (first middle), speed (second middle), and electromagnetic torque (bottom graph) for different levels of solar irradiance at 25°C

The transient performance of motor current and torque during solar irradiation step change in Figs. 11-12 is affected by the presence of the input/output filters.

Figs. 9-12 show that the developed torque under open-circuit drops to around 15% of that at $1000W^2m^{-2}$. Similarly, the speed and hence flow rate (6) drops to 40% of that at $1000W^2m^{-2}$.

Fig. 12 shows that the motor speed is less affected by solar irradiance variations during open-circuit fault. This scenario was predicted by (10).

V. CONCLUSION

The following conclusions can be drawn:

1. PV water pumping systems are the future trendsetter for providing eco-friendly water supply. As the PV systems experiences steadily reduction in cost, and rise in the efficiency.
2. The centrifugal pumps are well suited for PV water pumping system due to their operational and economical advantages.
3. The boost topology has ability of tracking MPP through simple and inexpensive MPPT. Moreover, this topology has the advantage of sustainable operation under faults albeit with reduced captured PV power and hence water flow rate. However, the boost topology suffers from high inrush current during start up, and a current limiting resistor should be incorporated in the circuit.

APPENDIX

$$a_3=V_{ao}L_aJ_aC_o,\ a_2=\left(I_{ino}(1-D_o)L_aJ_a+V_{ao}J_aR_a+V_{ao}L_a\left(B+2k_\omega\omega_o\right)\right),$$

$$a_1=\left(I_{ino}(1-D_o)\left(J_aR_a+L_a\left(B+2k_\omega\omega_o\right)\right)+V_{ao}\left(k_\Phi{}^2+J_a+R_a\left(B+2k_\omega\omega_o\right)\right)\right)$$

$$a_o=I_{ino}(1-D_o)\left(k_\Phi+R_a\left(B+2k_\omega\omega_o\right)\right)+V_{ao}\left(B+2k_\omega\omega_o\right)$$

$$b_4=L_aJ_aC_oL_{in},$$

$$b_3=\left(L_aJ_aC_ok_{pv}+L_{in}J_aR_a+L_{in}L_a\left(B+2k_\omega\omega_o\right)\right),$$

$$b_2=\begin{pmatrix} L_a J_a (1\text{-}D_o)^2+k_{pv} J_a R_a+k_{pv} L_a \left(B+2k_\omega \omega_o\right)+ \\ L_{in}\left(k_\Phi{}^2+J_a+R_a\left(B+2k_\omega \omega_o\right)\right) \end{pmatrix}$$

$$b_1=\begin{pmatrix} L_{in}\left(B+2k_\omega \omega_o\right)+L_{in}\left(k_\Phi{}^2+J_a+k_{pv}\left(B+2k_\omega \omega_o\right)\right)+ \\ (1\text{-}D_o)^2\left(J_a R_a+L_a\left(B+2k_\omega \omega_o\right)\right) \end{pmatrix}$$

$$b_o=(1\text{-}D_o)^2\left(k_\Phi+R_a\left(B+2k_\omega \omega_o\right)\right)+k_{pv}\left(B+2k_\omega \omega_o\right)$$

REFERENCES

[1] J. T. Bialasiewicz, "Renewable Energy System with Photovoltaic Power Generators: Operation and Modeling," *IEEE Transaction on Industry Electronics,* vol. 55, pp. 2752-2758, July 2008.

[2] J. T. Bialasiewicz and e. al, "Power-Electronics Systems for the Grid Integration of Renewable Energy Sources : A Survey " *IEEE Transaction on Industry Electronics,* vol. 53, pp. 1002-1016, August 2006.

[3] E. Endo and K. Kurokawa, "Sizing procedure for photovoltaic systems " i*n IEEE First World Conference on Photovoltaic Energy Conversion, 1994.*, pp. 1196-1199, 1994.

[4] Marcelo Gradella Villalva, Jonas Rafael Gazoli, and E. R. Filho, "Comprehensive Approach to Modeling and Simulation of Photovoltaic Arrays," *IEEE Transaction on Power Electronics*, vol. 24, pp. 1198-1208, 2008.

[5] P. Midya;, P. T. Krein;, R. J. Turnbull;, R. Reppa;, and J. Kimball;, "Dynamic Maximum Power Point Tracker for Photovoltaic Applications," *IEEE Transaction on Industry Electronics*, pp. 1710-1716, 1996.

[6] T. Esram and P. L. Chapman, "Comparison of Photovoltaic Array Maximum Power Point Tracking Techniques," *IEEE Transaction on Energy Conversion ,* vol. 22, pp. 439-779*, 2007.*

[7] A. Hadj Arab, F. Chenlo, K.Mukadam, and J. L. Balenzategui, "Performance of PV water pumping systems," *Renewable energy,* vol. 18, pp. 191-204, 1999.

[8] J.A. Roger, Theory of the direct coupling between DC motors and photovoltaic solar arrays", *Solar Energy*, pp. 193–198, 1979.

[9] W.R. Anis and H.M.B. Metwally, Dynamic performance of a directly coupled PV pumping system", Solar *Energy*, pp. 369–377,1994.

[10] J. Appelbaum, Starting and steady-state characteristics of DC motors powered by solar cell generators, *IEEE Transaction on Energy Conversion*, New York, NY EC-1,pp. 230-237, 1986 .

[11] A. A. Ghoeniem, "Design optimization of photovoltaic powered water pumping system," *Energy Conversion and Management* vol. 47, pp. 1449-1463, 2005.

[12] M. Alonso Abella, E. Loerenzo, and F. Chenlo, "PV Water Pumping Systems Based on Standard Frequency Converters," *Progress in Photovoltaic: Research and Applications*, vol. 11, pp. 179-191, 2002.